Volume 261, Issues 3–4 30 September 2007 ISSN 0012-821X

ELSEVIER

EARTH & PLANETARY SCIENCE LETTERS

Available online at www.sciencedirect.com
ScienceDirect
Earth and Planetary Science Letters 261 (2007) 443–455
EPSL
www.elsevier.com/locate/epsl

Influence of thermochemical piles on topography at Earth's core–mantle boundary

Teresa Mae Lassak [a,*], Allen K. McNamara [a], Shijie Zhong [b]

[a] School of Earth and Space Exploration, Arizona State University, Tempe, AZ 85287-1404, United States
[b] Department of Physics, University of Colorado, Boulder, CO 80309-0390, United States

Received 14 November 2006; received in revised form 18 June 2007; accepted 7 July 2007
Available online 18 July 2007
Editor: R.D. van der Hilst

Abstract

Numerous seismic studies reveal the presence of two large, low velocity anomalies beneath Africa and the central Pacific. Efforts to characterize these anomalies have yielded a variety of interpretations over the years, both isochemical and thermochemical. Previous interpretations have included large, isochemical superplumes, clusters of smaller thermal plumes, and doming thermochemical superplumes. A conceptual mantle model that is presently growing favor involves long-lived thermochemical piles. In anticipation that nutation studies will provide better topographic constraints on the core–mantle boundary (CMB) in the future, we examine the effects of thermochemical piles at this boundary. In this study, we perform numerical modeling of thermochemical and isochemical convection as a function of convective vigor and temperature-dependent viscosity to predict the topography at Earth's CMB. Our results show that in isochemical convection, downwellings always lead to negative (depressed) CMB topography, while upwellings cause positive (elevated) topography, consistent with previous studies. However, in thermochemical convection, CMB topography and its relationship to downwellings and thermochemical piles are significantly affected by temperature-dependent viscosity. For isoviscous or weakly temperature-dependent viscosity, the piles cause negative CMB topography, while positive topography is often below cold downwellings. However, for realistic, more strongly temperature-dependent viscosity, the most negative CMB topography is below downwellings, while the topography below the piles is often slightly more positive and/or flat, similar to upwellings in isochemical models. We also show that although thermochemical piles are intrinsically more dense, the large thermal buoyancy associated with them leads to overall relative buoyancy that is on par with slabs. Consequently, thermochemical models lead to an overall reduction in magnitude of CMB topography with respect to isochemical models.
Published by Elsevier B.V.

Keywords: CMB topography; mantle convection; tomography; mantle plumes

1. Introduction

Earth's lowermost mantle and the core–mantle boundary (CMB) are regions of intense interest and have been interpreted to have a high degree of structural complexity, both chemically and thermally (e.g., Lay et al., 1998; Montague et al., 1998; Garnero, 2000; Buffett et al., 2000). Of particular interest is the presence of two large, low-velocity anomalies detected beneath Africa and the central Pacific as observed in seismic tomography studies (Dziewonski, 1984; Su et al., 1994;

* Corresponding author. Tel./fax: +1 480 965 8102.
E-mail address: Teresa.Lassak@asu.edu (T.M. Lassak).

0012-821X/$ - see front matter. Published by Elsevier B.V.
doi:10.1016/j.epsl.2007.07.015

Li and Romanowicz, 1996; Masters et al., 1996; Grand et al., 1997; Su and Dziewonski, 1997; Breger and Romanowicz, 1998; Ritsema et al., 1999; Kuo et al., 2000; Masters et al., 2000; Gu et al., 2001; Romanowicz, 2001; Wen et al., 2001; Ni et al., 2002; Romanowicz and Gung, 2002; To. et al., 2005). Furthermore, there is observational evidence that these anomalies may be compositional in nature, hinting at possible chemically distinct lower mantle regions (Wysession, 1996a,b; Breger and Romanowicz, 1998; Kennett et al., 1998; Ritsema et al., 1999; Ishii and Tromp, 1999; van der Hilst and Karason, 1999; Masters et al., 2000; Romanowicz, 2001; Wen et al., 2001; Forte and Mitrovica, 2001; Luo et al., 2001; Romanowicz and Gung, 2002; Ritsema and van Heijst, 2002; Deschamps and Trampert, 2003; Ni and Helmberger, 2003a,b; Wang and Wen, 2004; Ishii and Tromp, 2004; Trampert et al., 2004; To. et al., 2005; Ford et al., 2006). This interpretation is supported by geochemical evidence that appears to require the presence of distinct chemical reservoirs in the mantle as source regions for ocean island basalts (OIBs) and mid-ocean ridge basalts (MORBs) (e.g., Hofmann, 1997).

Although there is growing evidence that the large seismic, low-velocity anomalies beneath Africa and the Pacific are thermochemical, we are not yet at a stage where we can conclusively exclude isochemical conceptual mantle models. As a result, efforts to characterize these anomalies have yielded a variety of interpretations, both isochemical and thermochemical. We note that an isochemical mantle model does not necessarily impose a lack of chemical heterogeneity, but rather that chemical heterogeneity does not play a role in the larger-scale mantle dynamics. Previous dynamical interpretations of these anomalies have included isochemical superplumes (e.g., Thompson and Tackley, 1998), clusters of smaller thermal plumes (Schubert et al., 2004; Ritsema et al., in press), and actively rising, doming thermochemical superplumes (e.g., Davaille, 1999; Davaille et al., 2002, 2003). Another mantle model, which we focus on here, involves long-lived thermochemical piles (e.g., Tackley, 1998; Kellogg et al., 1999; Hansen and Yuen, 2000; Tackley, 2000; Jellinek and Manga, 2002, 2004; McNamara and Zhong, 2005; Tan and Gurnis, 2005).

Many geodynamical studies, both experimental and numerical, have been performed to better understand the behavior of hypothetical thermochemical piles in the lower mantle as the source of the chemical heterogeneity observed at the surface and as the cause of the large, low-velocity anomalies observed seismically beneath Africa and the Pacific (e.g., Christensen and Hofmann, 1994; Tackley, 1998; Kellogg et al., 1999; Montague and Kellogg, 2000; Tackley, 2000; Ni et al., 2002; Jellinek and Manga, 2002, 2004; McNamara and Zhong, 2004a,b; McNamara and Zhong, 2005; Tan and Gurnis, 2005; Nakagawa and Tackley, 2005; Nakagawa and Tackley, 2006). Despite the existence of many proposed thermochemical pile models, a common characteristic in these models is that they involve an intrinsically more dense (~2–5%) mantle component that is passively swept along the base of the mantle away from regions of ancient subduction and accumulate into large piles in upwelling regions. Interpretations that hypothetical piles are located beneath Africa and the central Pacific (e.g., Davaille, 1999; Davaille et al., 2002, 2003; Jellinek and Manga, 2004; Tan and Gurnis, 2005) are supported by recent geodynamical predictions that incorporate Earth's plate history for the last 120 Myrs as surface boundary conditions in numerical thermochemical convection models (McNamara and Zhong, 2005). Akin to thermochemical superplume models (e.g., Davaille, 1999; Davaille et al., 2002, 2003), thermochemical piles are predicted to be a source region for thermal plumes which may rise from their peaks, entraining pile material as they ascend. This has been proposed as a feasible mechanism for explaining the different observed geochemistry of OIBs and MORBs (e.g., Davaille, 1999; Kellogg et al., 1999; Tackley, 2000; Davaille et al., 2002; Jellinek and Manga, 2002; Davaille et al., 2003; Jellinek and Manga, 2004).

While the idea of thermochemical piles is consistent with many aspects of the seismological and geochemical data, it remains a hypothetical, conceptual model subject to further testing and scrutiny. One possible avenue for further testing involves the study of variations in Earth's rotation (nutations) which may provide clues into the lowermost mantle structure and CMB topography (e.g., Dahlen, 1976; Gwinn et al., 1986; Wu and Wahr, 1997; Buffett et al., 2000; Mathews et al., 2002; Rost and Revenaugh, 2003; Sze and van der Hilst, 2003). We predict that ongoing and future nutation studies will show promise in providing constraints on CMB topography, which may help discern between the various proposed mantle models (e.g., Forte and Mitrovica, 2001).

Previous geodynamical work focusing on the effects of subducting slabs on stress or topography on the CMB in isochemical mantle models has clearly shown that downgoing slabs cause negative CMB topography (e.g., Hager and Richards, 1989). Furthermore, similar isochemical studies that have investigated the effects of thermal plumes on the geoid have shown that thermal plumes cause positive topography at the CMB (Hager

and Richards, 1989; King, 1997). It is difficult to intuitively surmise how the presence of thermochemical piles would affect CMB topography, compared to the isochemical mantle models. Although piles are intrinsically more dense, it should not be assumed that they would generally cause a downward CMB topographic depression beneath them. Rather, piles tend to be significantly hotter than the ambient mantle (e.g., Davaille, 1999; Kellogg et al., 1999; Tackley, 2000; Davaille et al., 2002; Jellinek and Manga, 2002; Davaille et al., 2003; Jellinek and Manga, 2004; McNamara and Zhong, 2004a,b; McNamara and Zhong, 2005), so the effective buoyancy of a pile reflects density contributions both from its intrinsic density and from the decreased density due to thermal expansivity.

In fact, if the effective density of a pile is similar to that of cold downwellings, then it is likely that piles will not necessarily lead to depressed CMB topography. The combination of slabs and piles could lead to a dramatic reduction of overall CMB topography, when compared to an isochemical mantle model. In addition, CMB stress magnitude is directly proportional to viscosity, and it is expected that low-viscosity, hot piles will produce lower stresses than higher-viscosity, cold downwellings.

The primary motivation for this work is to predict the effect of thermochemical piles on CMB topography, particularly in comparison to otherwise identical isochemical calculations. Isochemical mantle models highlight a clear relationship between slabs producing downward topography and plumes producing upward topography, however, we suggest that in thermochemical models, the density decrease in piles due to thermal expansivity acts to produce a net effective buoyancy that is similar to that of slabs. As a result, the presence of piles would reduce the magnitude of CMB topography, thereby acting as a buoyancy buffer near the CMB. It is crucial to test this hypothesis as we expect that future geodetic studies will help provide constraints on CMB topography and, consequently, will aid in our ability to distinguish between various mantle models.

2. Method

We perform numerical modeling of thermochemical and isochemical convection as a function of convective vigor and temperature-dependent viscosity in order to predict the stress and topography at Earth's CMB. We first describe calculations with relatively low convective vigor ($Ra=10^5$) to better understand the fundamental physics, and we next describe calculations that include a viscosity increase at the transition zone and have a higher, more mantle-consistent convective vigor ($Ra=10^7$). To illustrate the effects of viscosity on stress at the CMB we investigate various degrees of temperature-dependent viscosity. All calculations are performed in two dimensions using the finite element method, as implemented in Citcom (Moresi and Gurnis, 1996; Zhong et al., 2000). In this section, we will describe the necessary equations for calculating convection, rheology and stress.

2.1. Convection equations

The calculations are performed by solving the non-dimensionalized conservation of mass, momentum and energy equations using the Boussinesq approximation. Respectively, these equations are:

$$\nabla \cdot \boldsymbol{u} = 0 \tag{1}$$

$$-\nabla P + \nabla \cdot (\eta \dot{\varepsilon}) = (RaT - RbC)\,\hat{z} \tag{2}$$

$$\frac{\partial T}{\partial t} + (\boldsymbol{u}\cdot\nabla)T = \nabla(\kappa \cdot \nabla T) \tag{3}$$

where $\boldsymbol{u}$ is the velocity vector, P is the dynamic pressure, η is the non-dimensional viscosity, $\dot{\varepsilon}$ is the strain rate tensor, Ra is the thermal Rayleigh number, T is the temperature (which ranges from 0 to 1), Rb is the chemical Rayleigh number, C is the compositional coefficient (ranging from 0 to 1), t is time, and κ is thermal diffusivity.

The thermal Rayleigh number is defined as:

$$Ra = \frac{\rho_o g \alpha \Delta T h^3}{\eta_o \kappa_o} \tag{4}$$

where ρ_o is the reference density, g is gravity; α is the thermal expansivity, h is the mantle thickness, η_o is the reference viscosity, and κ_o is the reference thermal diffusivity.

Similarly, the chemical Rayleigh number is defined as:

$$Rb = \frac{\Delta \rho g h^3}{\eta_o \kappa_o} \tag{5}$$

where $\Delta\rho$ is the density difference between the two chemical components.

Consequently, the thermochemical dimensional equation of state is:

$$\rho = \rho_o[1 - \alpha(T - T_o)] + \Delta\rho C \tag{6}$$

For isochemical calculations, Eq. (6) simplifies to $\rho=\rho_o[1-\alpha(T-T_o)]$.

We utilize the ratio of chemical to thermal buoyancy using the non-dimensional quantity B, the buoyancy number, which is a measure of the intrinsic density contrast in the thermochemical model:

$$B = \frac{Rb}{Ra} = \frac{\Delta\rho}{\rho\alpha\Delta T} \tag{7}$$

2.2. Rheology

We employ a temperature-dependent rheology, and for the higher Rayleigh number cases, we employ depth-dependence. Following McNamara and Zhong (2004a), we use the following formulation for viscosity:

$$\eta(T) = \eta_r \exp[A(0.5 - T)] \tag{8}$$

where η_r represents the viscosity prefactor, A represents the activation coefficient that controls the temperature-dependence, and T is the temperature. For the lower Rayleigh number cases, η_r is simply 1, whereas for the higher Rayleigh number cases in which we employ the lower mantle viscosity increase, η_r is 1 above the 660 km phase transition, and η_r is 50 below the 660 km discontinuity. As evident in the formulation above, the Rayleigh number is defined by the viscosity at which the non-dimensional temperature is 0.5. We define, and use hereafter, the term "viscosity contrast" ($\Delta\eta = \exp[A]$) as a measure of temperature-dependence which represents the ratio of maximum to minimum possible viscosity.

2.3. Computational method

All calculations are performed in two dimensions using the finite element method, as implemented in Citcom (Moresi and Gurnis, 1996; Zhong et al., 2000). Using the method as described in McNamara and Zhong (2004a), we track compositional evolution via advection tracers by employing the ratio tracer method as reviewed and tested in Tackley and King (2003). The composition is uniform for each element as determined by the ratio of dense tracers to total number of tracers for that particular element. We use a predictor-corrector scheme to advect tracers, using an average of 16 particle tracers in each element. The model geometry has an aspect ratio of 6, and employs free-slip velocity boundary conditions on all boundaries. Thermal boundary conditions are constant and isothermal where $T=1$ along the lower boundary and $T=0$ along the upper boundary. The calculations were performed on a mesh with 97 vertical and 641 horizontal rectangular elements with increased resolution near the top 10% and the bottom 30% of the mesh. We performed resolution tests with both higher and lower numbers of elements to confirm that this resolution is more than adequate for this study.

All calculations started with a conductive initial temperature condition and were run for enough time such that the initial condition did not influence the results. Each thermochemical calculation was started with a flat, compositional layer and progressed until the thermochemical component was completely entrained, thereby ultimately reaching an isochemical state. The initial thermochemical layer thickness is 0.2 (20% of the mantle thickness). We investigated numerous buoyancy numbers, from those leading to stable, flat layers to those leading to quick overturns. For this study, we focused on those that led to long-lived thermochemical piles that exhibit significant topography.

2.4. Calculation of stress and topography at bottom boundary

We calculate the value of deviatoric stress at the bottom boundary of the model space using:

$$\sigma_{zz} = 2\eta\dot{\varepsilon}_{zz} - P, \tag{9}$$

where $\dot{\varepsilon}_{zz} = \frac{\partial w}{\partial z}$ is the strain rate, σ_{zz} is the deviatoric stress acting on the horizontal plane (the CMB) in the vertical direction and w is velocity in the vertical direction. For each step, we subtracted the horizontally-averaged stress such that the figures show only deviations from the average stress along the boundary. This is consistent with positive stress representing positive topography and negative stress representing negative topography. Positive topography is topography that is upward of the mean CMB elevation and negative topography is downward of the mean CMB elevation. Dimensional topography (δh) can be calculated from σ_{zz} using:

$$\delta h = \frac{\sigma_{zz\_cmb}}{\Delta\rho g} \tag{10}$$

where all variables are dimensional. σ_{zz_cmb} is the dimensional normal stress in vertical direction at the CMB, $\Delta\rho$ is the density contrast between Earth's mantle and core, and g is the gravitational acceleration at the CMB.

The calculated dimensional topography, while dependent upon the parameters in Eq. (10), is directly dependent on the dimensionalization of stress. In fact, the dimensionalization of stress is directly proportional to the dimensional reference viscosity value given in the Rayleigh number term ($\sigma_{\text{dimensional}} = \kappa_o\eta_o h^{-2}\sigma_{\text{non-dimensional}}$). As a

result, the calculated dimensional topography value derived in this work scales directly with the dimensional reference viscosity and Rayleigh number. Moreover, while we do calculate topography for the calculations with the more Earth-consistent rheological formulation (Cases 5 and 6), we find both non-dimensional stress and dimensional topography to be equivalent measures in the comparison between particular isochemical and thermochemical calculations because both expressions are linearly proportional to one another. In other words, the relative stress/topography when compared between different cases is robust, however the absolute number calculated for CMB topography should be considered with some caution.

3. Results

For each set of model parameters that we vary Ra and $\Delta\eta$, we present two calculations, one isochemical and one thermochemical. In actuality, we perform many more thermochemical calculations that span the range of buoyancy numbers from those that lead to a flat layer to those leading to quick, unstable overturns of the intrinsically more dense material. Of those, we select a representative case that leads to the formation of long-lived, stable piles. Table 1 lists the parameters used in each case.

We first present cases with the lower Rayleigh number ($Ra=10^5$). Snapshots in time of these calculations are presented in Fig. 1. In each of calculation snapshots, we show buoyancy minus the horizontal average of buoyancy normalized by Ra (defined as $[(RaT-RbC)-\langle RaT-RbC\rangle_{horz}]/Ra$) in the top panel, temperature in the second panel, composition (in the third panel for thermochemical calculations only), and lower boundary stress in the lowermost panel. We choose a sign convention such that negative stress leads to negative topography and positive stress leads to positive topography of the CMB. Again, positive topography is upward of the mean CMB elevation and negative topography is downward of the mean CMB elevation. Snapshots in the left column correspond to isochemical cases, and those in the right column refer to thermochemical cases. Each row of snapshots refers to a specific viscosity contrast.

Table 1
Catalogue of isochemical and thermochemical numerical experiments

Case	Fig	$\Delta\eta$	$\eta_{r(660)}$	Ra	B number	E
1A	1A	1	1	10^5	0.0	0.000
1B	1B	1	1	10^5	0.8	0.000
2A	1C	10^3	1	10^5	0.0	6.908
2B	1D	10^3	1	10^5	0.8	6.908
3A	1E	10^4	1	10^5	0.0	9.210
3B	1F	10^4	1	10^5	0.8	9.210
4A	2A	10^2	1	10^5	0.0	4.605
4B	2B–E	10^2	1	10^5	0.9	4.605
5A	3A	10^3	50	10^7	0.0	6.908
5B	3B	10^3	50	10^7	0.8	6.908
6A	4A	10^4	50	10^7	0.0	9.210
6B	4B–E	10^4	50	10^7	0.8	9.210

Thermochemical experiments were performed with a layer of initial thickness equivalent to 20% of the model height. $\Delta\eta$ is the viscosity contrast (the measure of temperature-dependence), $\eta_{r(660)}$ is the viscosity prefactor at the 660 km phase transition, Ra is the thermal Rayleigh number, and E is the activation coefficient.

Cases 1A (isochemical, Fig. 1A) and 1B (thermochemical, Fig. 1B) employ an isoviscous rheology ($\Delta\eta=1$). In Case 1A (Fig. 1A), CMB topography is negative beneath cool downwellings and is positive below hot upwelling plumes, consistent with previous geodynamical studies. It is obvious that this is related to the observed negative and positive buoyancy associated with downwellings and upwellings, respectively. Unlike Case 1A, downwellings in Case 1B (Fig. 1B), do not result in depressions along the lower boundary. The thermochemical piles are more negatively buoyant than slabs, and topography beneath them is negative, although at a significantly lower magnitude than that caused by the downwellings in the associated isochemical case.

The temperature-dependence of viscosity is increased ($\Delta\eta=10^3$) in Cases 2A (isochemical, Fig. 1C) and 2B (thermochemical, Fig. 1D). We note that in the cases with temperature-dependence of viscosity, the Rayleigh number is defined by the viscosity at a non-dimensional temperature of 0.5, as discussed in the methods section. As observed in Case 1A, the isochemical calculation in Case 2A displays negative topography beneath downwellings and positive topography beneath upwellings. However, there is a noticeable difference between the stresses predicted in isoviscous Case 1A and the temperature-dependent viscosity Case 2A. Whereas Case 1A exhibits positive and negative stresses, which are similar in magnitude, Case 2A clearly shows a disparity in stress magnitude between the larger negative stresses beneath downwellings and the smaller positive stresses beneath upwellings. The reduction in stress magnitude is likely because viscosity, which is proportional to stress, decreases with increasing temperature. In the thermochemical Case 2B (Fig. 1D), the thermochemical piles appear to have a buoyancy on par with the downwellings. Stress beneath the thermochemical piles can be classified as ubiquitously neither negative nor positive, resulting in an ambiguous relationship between the presence of a pile and its associated CMB topography. For example, positive topography is predicted for

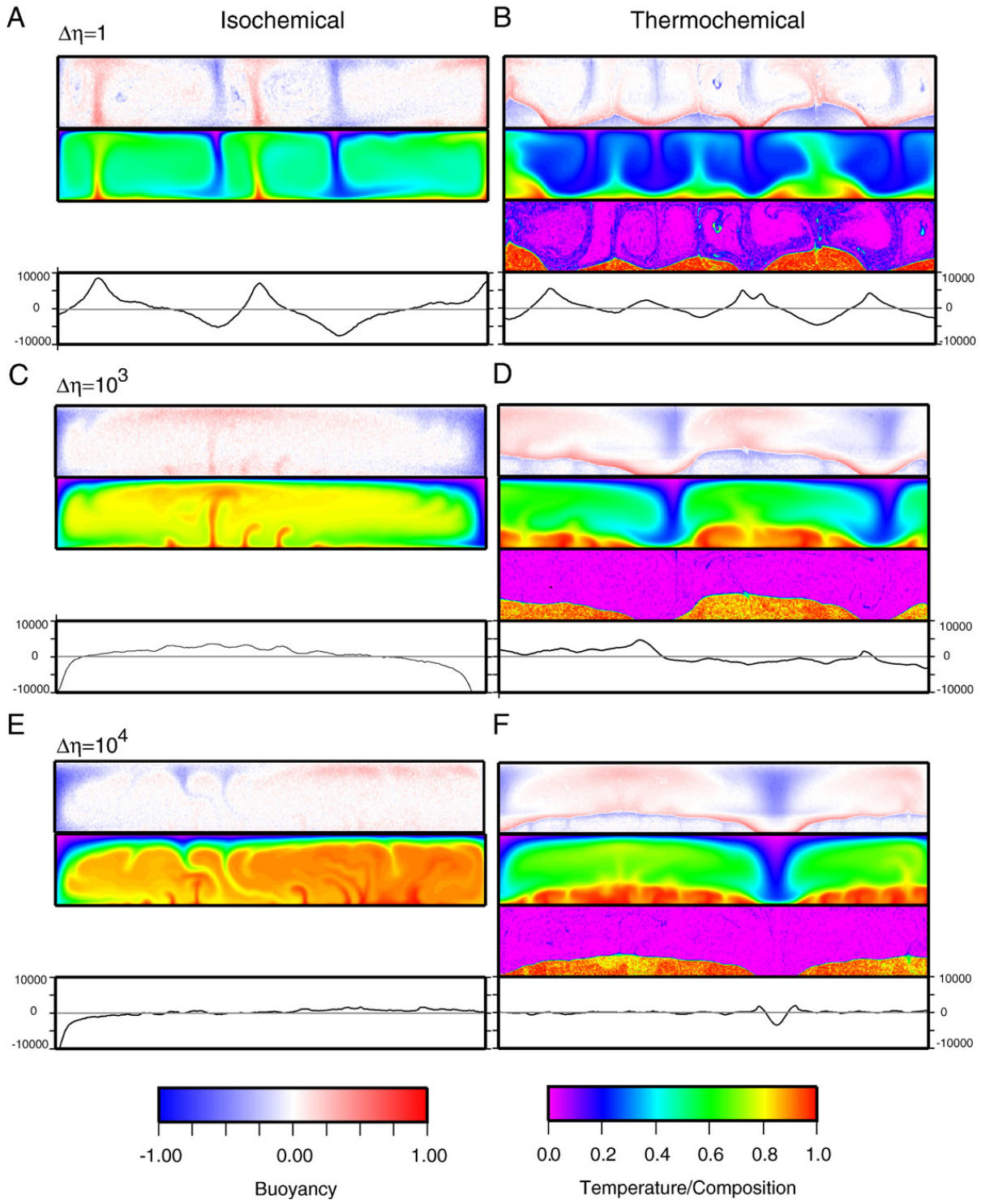

Fig. 1. Illustrated in this figure are isochemical and thermochemical convection calculations at a thermal Rayleigh number (10^5). Shown are calculations done at three temperature-dependent viscosity contrasts A) and B) $\Delta\eta = 10^3$, C) and D) $\Delta\eta = 10^3$, E) and F) $\Delta\eta = 10^4$. For each viscosity contrast, we show an isochemical (on the left) and a thermochemical (on the right) calculation timestep. We also, for each experiment, plot, buoyancy (top panel), temperature (second panel), composition (third panel, thermochemical experiment only) and stress (bottom panel).

the pile on the left, whereas negative topography is predicted for the other two piles.

The temperature-dependence of viscosity is further increased ($\Delta\eta = 10^4$) in Cases 3A (isochemical, Fig. 1E) and 3B (thermochemical, Fig. 1F). The increase in viscosity contrast leads to a more-rigid cold upper thermal boundary layer, resulting in much larger wavelength flow patterns. As observed in Case 2A, Case 3A also predicts

large negative topography beneath the downwellings and low-magnitude positive topography beneath the upwellings. In Case 3B (Fig. 1F), negative topography is predicted beneath one of the downwellings, while topography beneath the thermochemical piles remains relatively flat. The overall magnitude of the negative topography is reduced in magnitude in the thermochemical calculations, as compared to the isochemical calculations.

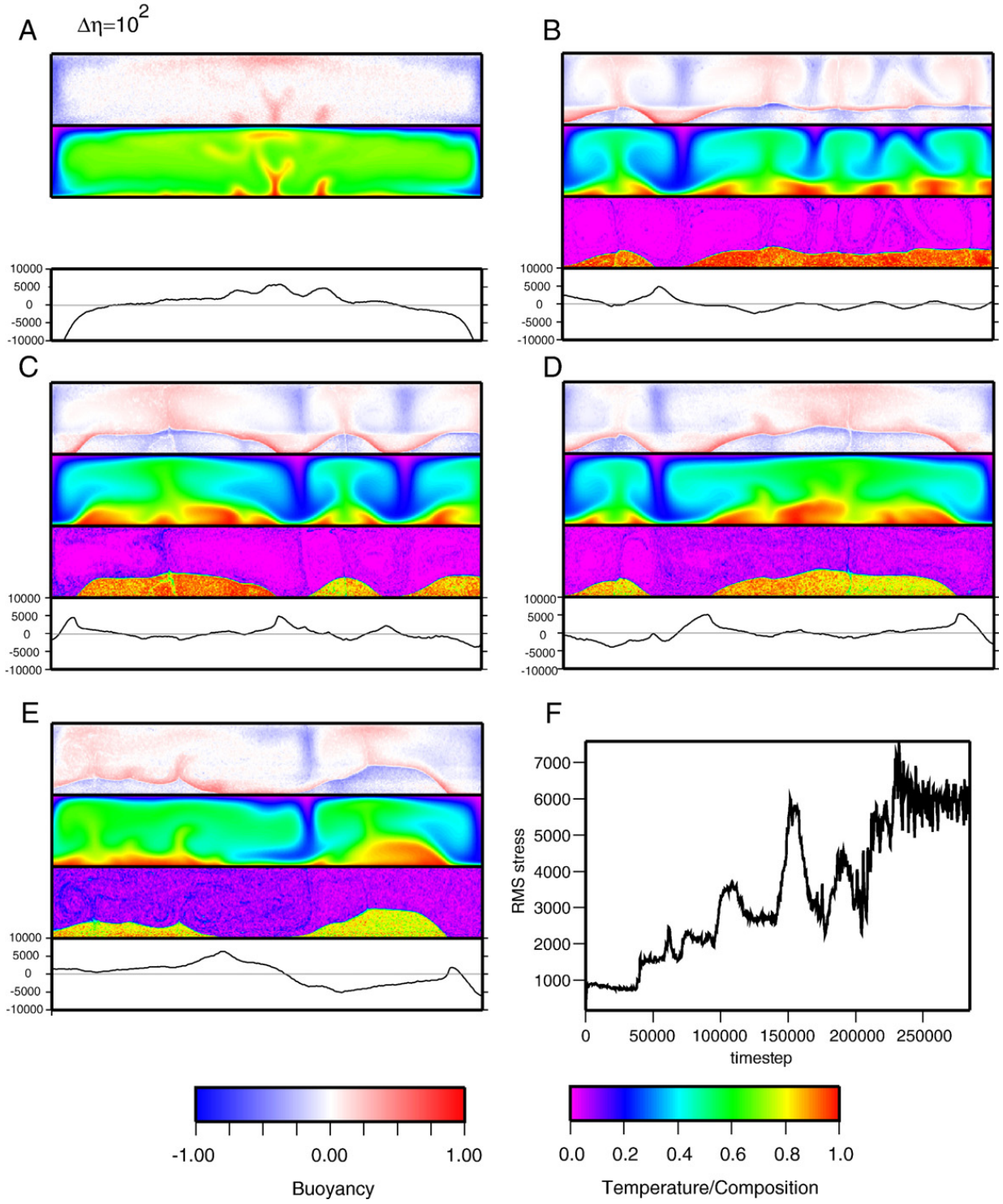

Fig. 2. Illustrated in this figure are thermochemical convection calculations at thermal $Ra=10^5$. Shown are calculations for a viscosity contrast of $\Delta\eta=10^2$. We show A) an isochemical calculation timestep, thermochemical calculation timesteps at B) 60,000, C) 90,000, D) 122,000, E) 162,000, and F) the root-mean squared (RMS) values of stress versus timestep. Observations in the isochemical calculations are similar to those for Fig. 1. As the calculation evolves, the piles become relatively more buoyant than slabs. F) Illustrates the evolution of stress variations with time evolution.

In Case 4 ($\Delta\eta=10^2$) (Fig. 2), we present a snapshot of an isochemical calculation along with a series of snapshots showing the evolution of its associated thermochemical calculation as the thermochemical piles become effectively less dense due to entrainment (a common characteristic of all thermochemical calculations). As observed in the other isochemical cases, Case 4A (Fig. 2A) has downwellings that produce negative topography whereas upwellings produce positive topography. For the thermochemical Case 4B, we show multiple timesteps (Fig. 2B–E). At the earliest time shown (Fig 2B), we observe both positive and negative topography beneath a single large pile (the one on the right). This topography is directly correlated to internal convection within the pile, where internal upwelling corresponds to positive topography and internal downwellings corresponds to negative topography. Throughout the calculation, some piles are marked with positive topography beneath them, whereas in others, negative topography is predicted. Again, there is no clear relationship between the presence of a pile and the direction of topography deflection beneath it. One interesting aspect that we notice however, as the effective density of a thermochemical pile decreases, the magnitude of CMB stress increases. Fig. 2F illustrates the evolution of the root-mean squared (RMS) value of stress as the calculation progresses. Essentially, as the calculation evolves, the thermochemical calculation effectively becomes more isochemical, and the overall magnitude of stress increases (Fig. 2F).

For the cases with a more Earth-consistent convective vigor ($Ra=10^7$) and a viscosity profile which includes a 50× increase at the 660 km phase transition, we investigate two different viscosity contrasts, 10^3 (Fig. 3) and 10^4 (Fig. 4). We convert stress to dimensional CMB topography in these calculations. Case 5A is an isochemical calculation with $\Delta\eta=10^3$ (Fig. 3A). Akin to the other isochemical cases, downwellings lead to negative topography and upwellings lead to positive topography. Notice that the model topography is unrealistically large (Gwinn et al., 1986; Wu and Wahr, 1997) with an amplitude of tens of kilometers, suggesting that our Rayleigh number is still too low compared with the Earth. In the thermochemical Case 5B with $\Delta\eta=10^3$ (Fig. 3B) we observe an overall decrease in topography magnitude along the lower boundary, compared to the isochemical case. The most negative topography occurs beneath one downwelling, whereas the topography elsewhere in the snapshot is relatively flat.

The effects of increasing the temperature-dependence ($\Delta\eta=10^4$) are illustrated in Case 6 (Fig. 4). Fig. 4 is setup similarly to Fig. 2, in which we show a snapshot from the isochemical calculation, and a series of snapshots showing the evolution of the thermochemical

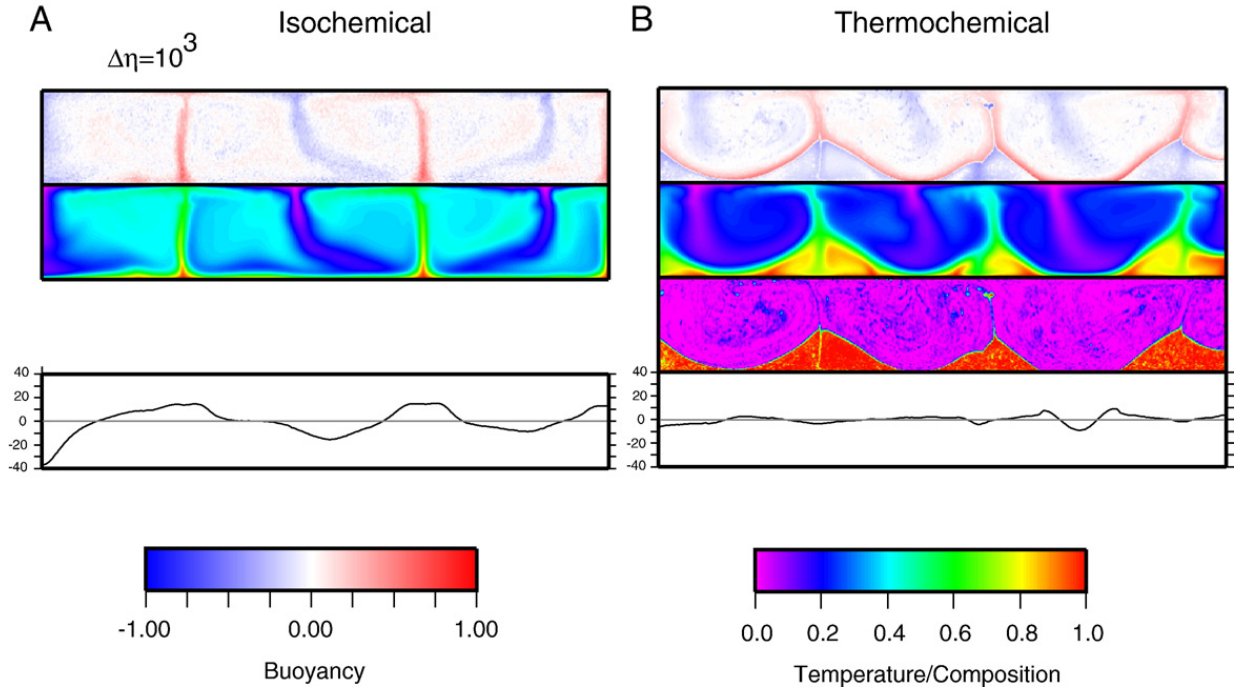

Fig. 3. Illustrated in this figure are thermochemical convection calculations at high thermal $Ra=10^7$ with a viscosity profile which includes a 50× increase at the 660 km phase transition. Shown are calculations done at a viscosity contrast: $\Delta\eta=10^3$. As in Fig. 1, we show an A) isochemical and a B) thermochemical calculation timestep. In these experiments, we convert stress to dimensional CMB topography. The topography is represented in the bottom panel in this figure and in Fig. 4. Topography values are in kilometers.

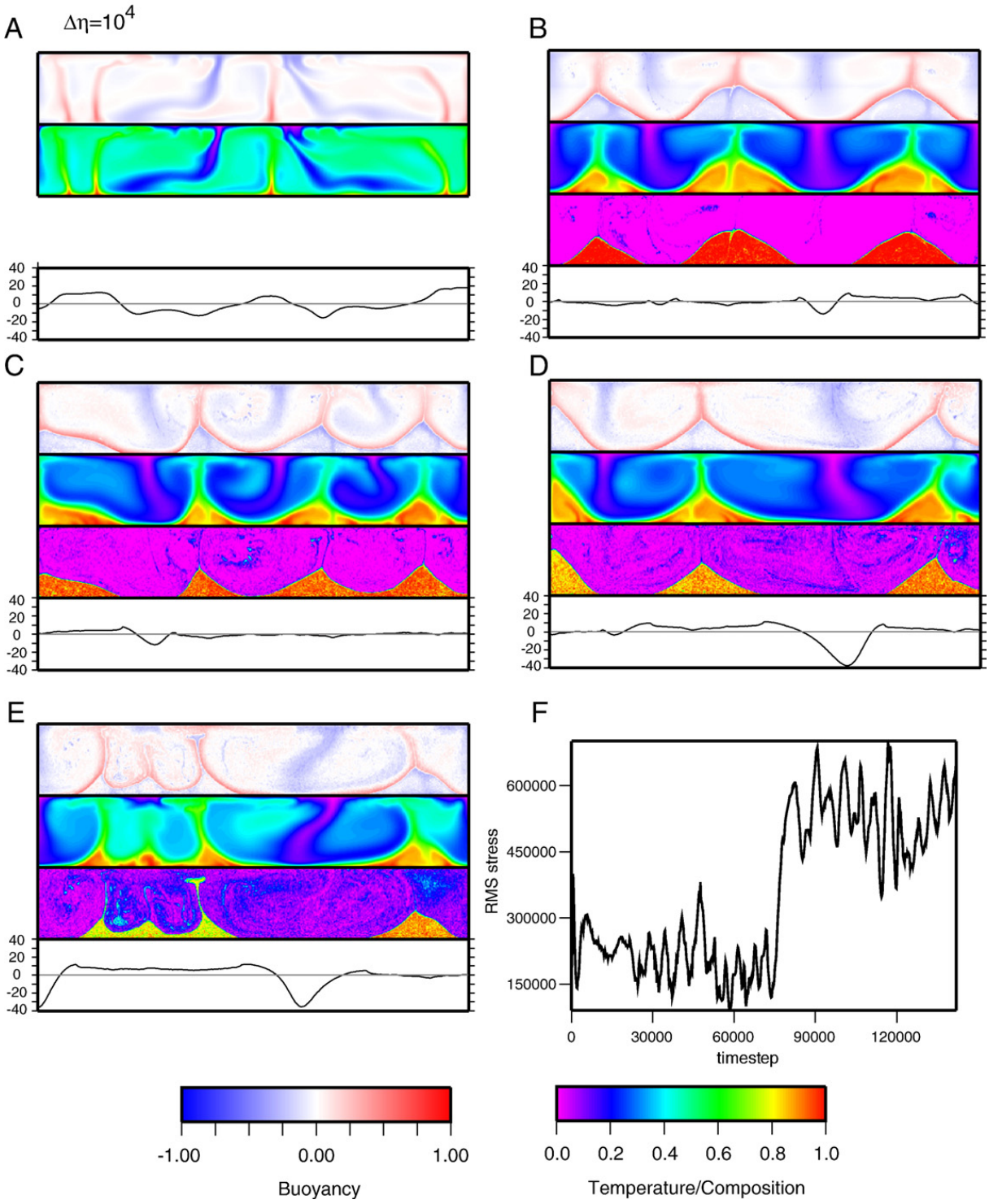

Fig. 4. Illustrated in this figure are thermochemical convection calculations at thermal $Ra=10^7$. Shown are calculations for a viscosity contrast of $\Delta\eta=10^4$. We show A) an isochemical calculation timestep, thermochemical calculation timesteps at B) 14,000, C) 60,000, D) 80,000, E) 107,400, and F) the root-mean squared (RMS) values of stress versus timestep.

calculation In the isochemical Case 6A (Fig. 2A), as in previous isochemical cases, we observe negative topography beneath downwellings and positive topography beneath upwellings. As with Case 5B, in Case 6B (Fig. 4B–E), topography beneath the piles tends to be flat, relative to the negative topography beneath some of the downwellings. As the calculation evolves, the effective density contrast between piles and surrounding mantle is reduced due to entrainment, and as a result, the downwellings become the most negatively buoyant

features and the magnitude of the topography beneath them increases. As in Case 4, we calculated the RMS of stress as a function of time (Fig. 4F), and we observe that as the effective density contrast of piles decreases and downwellings become more negatively buoyant than piles (Fig. 4D and E), overall topography increases in magnitude. Again, as the calculation evolves, the style and magnitude of deflection on the CMB begins to resemble that predicted for isochemical convection.

4. Discussion

The motivation for this study was to determine how the presence of thermochemical piles might affect deflection along the CMB as compared to isochemical convection. This is important to understand given that future geodetic studies may be used to place constraints on a conceptual model for the mantle. From this study, as well as from previous geodynamical studies, it is clear that for isochemical convection, negative topography is predicted beneath downwellings and positive topography is predicted beneath upwellings. In addition, the magnitude of stress (and hence topography) is proportional to the viscosity, such that cold, viscous downwellings lead to a larger amount of CMB deflection than do the hot, less-viscous upwellings. These characteristics observed in isochemical convection appear to be universal, and we have not observed any results contrary to this.

An important observation from this study is that temperature-dependence of viscosity plays a large role, and therefore, must be used in studies that determine stress/topography at any boundary. In the isoviscous ($\Delta\eta=1$) thermochemical cases, piles tend to have a stronger influence on CMB topography, whereas, for temperature-dependent viscosity, this is significantly reduced. For example, the isoviscous thermochemical Case 1B always exhibits negative topography beneath piles. However, in thermochemical cases with relatively strong temperature-dependent rheology (e.g. Cases 3B, 5B and 6B) the most negative topography is beneath downwellings, while the piles lead to slightly positive, flat CMB topography, similar to that from isochemical models. The thermochemical piles are hotter than the surrounding mantle, and therefore, less viscous. This in turns reduces the stress that the piles may cause at the CMB. The cold downwellings with high viscosity, on other hand, tend to impart more stress or depression at the CMB. This is analogous to the isochemical cases (e.g., Case 3A) in which upwellings (downwellings) have a much smaller (larger) effect on CMB topography as temperature-dependence of viscosity is increased. In short, our results indicate that if themochemical piles exist in the lower mantle with temperature-dependent viscosity, we do not expect, in general, to see negative CMB topography associated with them.

We find that these results are consistent with thermochemical piles providing a "buoyancy buffer" above the CMB. As intuitively observed in the isochemical cases, the negative and positive topography beneath downwellings and upwellings, respectively, can be directly correlated to the clear differences in buoyancy between the two. In the thermochemical models, on the other hand, the relationship between upwellings, downwellings, and piles with CMB topography is significantly less clear. In thermochemical models, if the intrinsic density of the thermochemical material is too high (high B), then piles fail to form at all. Moreover, if the intrinsic density is too low (low B), the thermochemical material either quickly overturns or it is rapidly entrained into the surrounding mantle. In fact, large, long-lived, stable piles exist only for a relatively narrow range of intrinsic density contrasts ($\sim$2–5%), and furthermore, we find that piles exist only when their effective buoyancy is similar to that of downwellings. Based on our results as well as previous work, we propose that this is a necessary buoyancy condition required for piles to form because it is the flow field caused by the more negative buoyancy of the downwellings that pushes thermochemical material away from downwelling regions. As a consequence, the variation of horizontal buoyancy in thermochemical pile models tends to be minimal compared to isochemical models, and that is the likely cause of the overall reduction in stress/topography magnitude observed in our results as compared to isochemical models. An equivalent explanation for this is that in thermochemical convection, the buoyancy from the upper part of the mantle is partially compensated at the compositional boundary, as evidenced by the large undulations at the boundary, thus reducing topography at the CMB.

By examining the thermochemical calculations at different times in their evolution and by plotting the RMS stress/topography as a function of time, we can observe how different effective density contrasts between piles and surrounding mantle affects the CMB topography (Figs. 2 and 4). This is because entrainment reduces this density contrast over time, and this is effectively analogous to studying different buoyancy numbers. As a thermochemical calculation evolves, the CMB stress/topography more resembles that of an isochemical calculation as the piles become more effectively less dense. As a result, downwellings produce stronger CMB deflection and the overall topography magnitude increases.

Experimental and theoretical works on the post-perovskite phase (Shim et al., 2001; Oganov and Ono, 2004; Hirose and Fujita, 2005) indicate that post-perovskite may exist in cooler regions of the lower mantle (e.g., downwellings) and may be important to include in future studies. Since post-perovskite is thought to be denser than perovskite, its presence in downwellings regions at the CMB could magnify the negative topography found in these regions of our study. Therefore, we predict that incorporating post-perovskite into our study would provide results consistent with those presented in our study.

In closing, our strongest result from this study is that for a mantle with high temperature-dependent viscosity, the basic characteristics of CMB topography from thermochemical convection models are rather similar to those from isochemical models. Therefore, an observation of either a null or a slightly positive topography on the CMB under a proposed pile region cannot credibly be used to refute the existence of the pile.

5. Conclusions

The primary goal of this work is to determine how proposed thermochemical piles in the lower mantle affect CMB topography, particularly in comparison to isochemical mantle models. From this and previous studies, we have found that in isochemical mantle models, there is a clear relationship between upwellings and downwellings to CMB topography in which downwellings lead to negative CMB topography and upwellings lead to positive topography. We find that this relationship is not so straightforward in thermochemical models that have long-lived, stable piles. In fact, we find that temperature-dependence of rheology plays a major role in how thermochemical piles affect CMB topography. At a relatively low degree of temperature-dependence, there is no clear correlation between piles and topography where some piles lead to positive topography and others lead to negative. In the Earth's mantle, we expect a much higher degree of temperature-dependence, and we find that in higher viscosity contrast cases ($\Delta\eta > 10^2$) the CMB topography beneath piles can be considered relatively flat. Downwellings, in these cases, result in negative CMB topography, not piles.

In these models, thermochemical piles have a buoyancy similar to that of the downwellings and may act as a buffer to buoyancy contrasts. Although thermochemical piles may be intrinsically more dense, it is important to emphasize that their effective density is significantly reduced by the density reduction associated with thermal expansion. It is likely that the negative buoyancy of the thermochemical piles is compensating negative slab buoyancy. As a result, we find that thermochemical models tend to result in a much lower overall CMB stress/topography than do their isochemical counterparts.

In general, thermochemical convection with temperature-dependent rheology does not lead to negative CMB topography beneath piles. In fact, cool downwellings appear to cause the most negative CMB topography. As a result, observations interpreted as positive topography beneath proposed piles cannot be used to discriminate between isochemical and thermochemical mantle models.

Acknowledgements

National Science Foundation grant EAR-0510383, EAR-0456356, EAR 0538255 and the David and Lucile Packard Foundation provided funds for this research. We also extend our gratitude to Scott King for providing us with guidance in topography calculation. In addition, we thank Thorsten Becker, Amanda Clark, Matt Fouch, Ed Garnero, Jim Tyburczy, and Meghan Graham for fruitful discussions. Finally, we thank an anonymous reviewer for the helpful suggestions that improved the manuscript.

References

Breger, L., Romanowicz, B., 1998. Three-dimensional structure at the base of the mantle beneath the central Pacific. Science 282, 718–720.

Buffett, B.A., Garnero, E.J., Jeanloz, R., 2000. Sediments at the top of Earth's core. Science 290, 1338–1342.

Christensen, U.R., Hofmann, A.W., 1994. Segregation of subducted oceanic-crust in the convecting mantle. J. Geophys. Res. 99 (B10), 19867–19884.

Dahlen, F.A., 1976. Passive influence of oceans upon rotation of Earth. Geophys. J. R. Astron. Soc. 46 (2), 363–406.

Davaille, A., 1999. Simultaneous generation of hotspots and superswells by convection in a heterogeneous planetary mantle. Nature 402, 756–760.

Davaille, A., Girard, F., Le Bars, M., 2002. How to anchor hotspots in a convecting mantle? Earth Planet. Sci. Lett. 203, 621–634.

Davaille, A., Le Bars, M., Carbonne, C., 2003. Thermal convection in a heterogeneous mantle. Geoscience 335, 141–156.

Deschamps, F., Trampert, J., 2003. Mantle tomography and its relation to temperature and composition. Phys. Earth Planet. Inter. 140, 277–291.

Dziewonski, A.M., 1984. Mapping the lower mantle — determination of lateral heterogeneity in P-velocity up to degree and order-6. J. Geophys. Res. 89 (B7), 5929–5952.

Ford, S.R., Garnero, E.J., McNamara, A.K., 2006. A strong lateral shear velocity gradient and anisotropy heterogeneity in the lowermost mantle beneath the southern Pacific. J. Geophys. Res. 111 (B3) (Art. No. B03306).

Forte, A.M., Mitrovica, J.X., 2001. Deep-mantle high viscosity flow and thermochemical structure inferred from seismic and geodynamic data. Nature 410, 1049–1056.

Garnero, E.J., 2000. Heterogeneity of the lowermost mantle. Annu. Rev. Earth Planet. Sci. 28, 509–537.

Grand, S.P., van der Hilst, R.D., Widiyantoro, S., 1997. Global seismic tomography: a snapshot of convection in the Earth. GSA Today 7 (4), 1–7.

Gu, Y.J., Dziewonski, A.M., Su, W.J., Ekstrom, G., 2001. Models of the mantle shear velocity and discontinuities in the pattern of lateral heterogeneities. J. Geophys. Res. 106 (B6), 11169–11199.

Gwinn, C.R., Herring, T.A., Shapiro, I.I., 1986. Geodesy by radio interferometry—studies of the forced nutations of the Earth. J. Geophys. Res. 91 (B5), 4755–4765.

Hager, B.H., Richards, M.A., 1989. Long-wavelength variations in Earth's geoid: physical models and dynamical implications. Philos. Trans. R. Soc. Lond., A 328, 309–327.

Hansen, U., Yuen, D., 2000. Extended-Boussinesq thermal-chemical convection with moving heat sources and variable viscosity. Earth Planet. Sci. Lett. 176, 401–411.

Hirose, K., Fujita, Y., 2005. Clapeyron slope of the post-perovskite phase transition in CaIrO3. Geophys. Res. Lett. 32, L13313. doi:10.1029/2005GL023219.

Hofmann, A.W., 1997. Mantle geochemistry: the message from oceanic volcanism. Nature 385, 219–229.

Ishii, M., Tromp, J., 1999. Normal-mode and free-air gravity constraints on lateral variations in velocity and density of Earth's mantle. Science 285, 1231–1236.

Ishii, M., Tromp, J., 2004. Constraining large-scale mantle heterogeneity using mantle and inner-core sensitive normal modes. Phys. Earth Planet. Inter. 146, 113–124.

Jellinek, A.M., Manga, M., 2002. The influence of a chemical boundary layer on the fixity, spacing, and lifetime of mantle plumes. Nature 418, 760–763.

Jellinek, A.M., Manga, M., 2004. Links between long-lived hot spots, mantle plumes, D″, and plate tectonics. Rev. Geophys. 42 (2003RG000144).

Kellogg, L.H., Hager, B.H., van der Hilst, R.D., 1999. Compositional stratification in the deep mantle. Science 283, 1881–1884.

Kennett, B.L.N., Widiyantoro, S., van der Hilst, R.D., 1998. Joint seismic tomography for bulk sound and shear wave speed in the Earth's mantle. J. Geophys. Res. 103 (B6), 12,469–12,493.

King, S.D., 1997. Geoid and topographic swells over temperature-dependent thermal plumes in spherical-axisymmetric geometry. Geophys. Res. Lett. 24 (23), 3093–3096.

Kuo, B.Y., Garnero, E.J., Lay, T., 2000. Tomographic inversion of S-SKS times for shear velocity heterogeneity in D″: degree 12 and hybrid models. J. Geophys. Res. 105 (B12), 28139–28157.

Lay, T., Williams, Q., Garnero, E.J., 1998. The core–mantle boundary layer and deep Earth dynamics. Nature 392, 461–468.

Li, X.D., Romanowicz, B., 1996. Global mantle shear velocity model developed using nonlinear asymptotic coupling theory. J. Geophys. Res. 101 (B10), 22245–22272.

Luo, S.-N., Ni, S., Helmberger, D.V., 2001. Evidence for a sharp lateral variation of velocity at the core–mantle boundary from multipathed PKPab. Earth Planet. Sci. Lett. 189, 155–164.

Masters, G., Johnson, S., Laske, G., Bolton, H., 1996. A shear-velocity model of the mantle. Philos. Trans. R. Soc. Lond., A 354, 1385–1411.

Masters, G., Laske, G., Bolton, H., Dziewonski, A.M., 2000. The relative behavior of shear velocity, bulk sound speed, and compressional velocity in the mantle: implications for chemical and thermal structure. In: Karato, S., Forte, A.M., Liebermann, R.C., Masters, G., Stixrude, L. (Eds.), Earth's Deep Interior: Mineral Physics and Tomography from the Atomic to the Global Scale. American Geophysical Union, Washington, D.C., USA, pp. 63–87.

Mathews, P.M., Herring, T.A., Buffett, B.A., 2002. Modeling of nutation and precession: new nutation series for nonrigid Earth and insights into the Earth's interior. J. Geophys. Res. 107 (B4). doi:10.1029/2001JB000390.

McNamara, A.K., Zhong, S., 2004a. The influence of thermochemical convection on the fixity of mantle plumes. Earth Planet. Sci. Lett. 222, 485–500.

McNamara, A.K., Zhong, S., 2004b. Thermochemical structures within a spherical mantle: superplumes or piles? J. Geophys. Res. 109. doi:10.1029/2003JB002847.

McNamara, A.K., Zhong, S., 2005. Thermochemical piles under Africa and the Pacific. Nature 437. doi:10.1038/nature04066.

Montague, N.L., Kellogg, L.H., 2000. Numerical models of a dense layer at the base of the mantle and implications for the geodynamics at D. J. Geophys. Res. 105, 11101–11114.

Montague, N.L., Kellogg, L.H., Manga, M., 1998. High Rayleigh number thermo-chemical models of a dense boundary layer in D″. Geophys. Res. Lett. 25 (13), 2345–2348.

Moresi, L., Gurnis, M., 1996. Constraints on the lateral strength of slabs from three-dimensional dynamic flow models. Earth Planet. Sci. Lett. 138, 15–28.

Nakagawa, T., Tackley, P.J., 2005. The interaction between the post-perovskite phase change and thermo-chemical boundary layer near the core–mantle boundary. Earth Planet. Sci. Lett. 238, 204–216.

Nakagawa, T., Tackley, P.J., 2006. Three-dimensional structures and dynamics in the deep mantle: effects of post-perovskite phase change and deep mantle layering. Geophys. Res. Lett. 33. doi:10.1029/2006GL025719.

Ni, S., Helmberger, D., 2003a. Seismological constraints on the South African superplume: could be oldest distinct structure on Earth. Earth Planet. Sci. Lett. 206, 119–131.

Ni, S., Helmberger, D., 2003b. Further constraints on the African superplume structure. Phys. Earth Planet. Inter. 140, 243–251.

Ni, S., Tan, E., Gurnis, M., Helmberger, D., 2002. Sharp sides to the African superplume. Science 296, 1850–1852.

Oganov, A.R., Ono, S., 2004. Theoretical and experimental evidence for a post-perovskite phase of $MgSiO_3$ in Earth's D″ layer. Nature 430, 445–448.

Ritsema, J., van Heijst, H.J., 2002. Constraints on the correlation of P- and S-wave velocity heterogeneity in the mantle from P, PP, PPP and PKPab traveltimes. Geophys. J. Int. 149 (2), 482–489.

Ritsema, J., van Heijst, H.J., Woodhouse, J.H., 1999. Complex shear wave velocity structure imaged beneath Africa and Iceland. Science 286 (5446), 1925–1928.

Ritsema, J., McNamara, A.K., Bull, A.L., in press. Tomographic filtering of geodynamical models, J. Geophys. Res. 112, B01303. doi:10.1029/2006JB004566.

Romanowicz, B., 2001. Can we resolve 3D density heterogeneity in the lower mantle? Geophys. Res. Lett. 28 (6), 1107–1110.

Romanowicz, B., Gung, Y., 2002. Superplumes from the core–mantle boundary to the lithosphere: implications for heat flux. Science 296, 513–516.

Rost, S., Revenaugh, J., 2003. Small-scale ultra-low velocity zone structure imaged by ScP. J. Geophys. Res. 108 (B1). doi:10.1029/2001JB001627.

Schubert, G., Masters, G., Olson, P., Tackley, P., 2004. Superplumes or plume clusters? Phys. Earth Planet. Inter. 146, 147–162.

Shim, S.H., Duffy, T.S., Shen, G.Y., 2001. Stability and structure of $MgSiO_3$ perovskite to 2300-kilometer depth in Earth's mantle. Science 293, 2437–2440.

Su, W.-J., Dziewonski, A.M., 1997. Simultaneous inversion for 3-D variations in shear and bulk velocity in the mantle. Phys. Earth Planet. Inter. 100, 135–156.

Su, W.J., Woodward, R.L., Dziewonski, A.M., 1994. Degree-12 model of shear velocity heterogeneity in the mantle. J. Geophys. Res. 99 (B4), 6945–6980.

Sze, E.K.M., van der Hilst, R.D., 2003. Core mantle boundary topography from short period PcP, PKP, and PKKP data. Phys. Earth. Planet. Inter. 135, 27–46.

Tackley, P.J., 1998. Three-dimensional simulations of mantle convection with a thermochemical CMB boundary layer: D″? In: Gurnis, M., Wysession, M.E., Knittle, E., Buffett, B.A. (Eds.), The Core–Mantle Boundary Region, Geodynamic Ser., vol. 28. AGU, Washington, D.C., pp. 231–253.

Tackley, P.J., 2000. Mantle convection and plate tectonics: toward an integrated physical and chemical theory. Science 288, 2002–2007.

Tackley, P.J., King, S.D., 2003. Testing the tracer ratio method for modeling active compositional fields in mantle convection simulations. Geochem. Geophys. Geosyst. 4. doi:10.1029/2001GC000214.

Tan, E., Gurnis, M., 2005. Metastable superplumes and mantle compressibility. Geophys. Res. Lett. 32 (20). doi:10.1029/2005GL024190.

Thompson, P.F., Tackley, P.J., 1998. Generation of mega-plumes from the core–mantle boundary in a compressible mantle with temperature-dependent viscosity. Geophys. Res. Lett. 25 (11), 1999–2002.

To., A., Romanowicz, B., Capdeville, Y., Takeuchi, N., 2005. 3D effects of sharp boundaries at the borders of the African and Pacific superplumes: observation and modeling. Earth Planet. Sci. Lett. 233, 137–153.

Trampert, J., Deschamps, F., Resovsky, J., Yuen, D., 2004. Probabilistic tomography maps chemical heterogeneities throughout the lower mantle. Science 306, 853–856.

van der Hilst, R.D., Karason, H., 1999. Compositional heterogeneity in the bottom 1000 kilometers of Earth's mantle: toward a hybrid convection model. Science 283, 1885–1888.

Wang, Y., Wen, L., 2004. Mapping the geometry and geographic distribution of a very low velocity province at the base of the Earth's mantle. J. Geophys. Res. 109. doi:10.1029/2003JB002674.

Wen, L., Silver, P., James, D., Kuehnel, R., 2001. Seismic evidence for a thermo-chemical boundary at the base of the Earth's mantle. Earth Planet. Sci. Lett. 189, 141–153.

Wysession, M.E., 1996a. Continents of the core. Nature 381, 373–374.

Wysession, M.E., 1996b. Large-scale structure at the core–mantle boundary from diffracted waves. Nature 382, 244–248.

Wu, X.P., Wahr, J.M., 1997. Effects of non-hydrostatic core–mantle boundary topography and core dynamics on Earth rotation. Geophys. J. Int. 128, 18–42.

Zhong, S., Zuber, M.T., Moresi, L., Gurnis, M., 2000. Role of temperature-dependent viscosity and surface plates in spherical shell models of mantle convection. J. Geophys. Res. 105, 11063–11082.